78-514

Buckling of Imperfect Anisotropic Circular Cylinders under Combined Loading

M. Booton*
Memorial University of Newfoundland, St. John's, Newfoundland, Canada
and
R. C. Tennyson†
University of Toronto, Toronto, Ontario, Canada

This study consisted of a theoretical and experimental investigation of the buckling of circular cylindrical shells under the simultaneous action of torsion, external pressure, and axial compression. Laminated anisotropic behavior was considered, as was the effect of small axisymmetric shape imperfections. The theoretical analysis took into account the exact form of the boundary conditions and nonlinear prebuckling deformations. Interactive stability surfaces were computed for a variety of laminate configurations together with approximate formulas for buckling under these three loading conditions. Comparisons with experimental data obtained from buckling tests on glass/epoxy cylinders were also made.

Nomenclature

A_{ij}, A^* = $\Sigma_k (\bar{Q}_{ij})_k (h_k - h_{k-1})$, $\{A_{ij}\}^{-1}$
B_{ij}, B^* = $\frac{1}{2}\Sigma_k (\bar{Q}_{ij})_k (h_k^2 - h_{k-1}^2)$, $-\{A_{ij}\}^{-1}\{B_{ij}\}$
D_{ij} = $\frac{1}{3}\Sigma_k (\bar{Q}_{ij})_k (h_k^3 - h_{k-1}^3)$
D^* = $\{D_{ij}\} - \{B_{ij}\}\{A_{ij}\}^{-1}\{B_{ij}\}$
E_{11}, E_{22}, G_{12} = orthotropic lamina moduli
h_k = thickness of kth lamina
K = q/q_0
k = R_s/R_x
L = cylinder length
M_x, M_y, M_{xy} = stress couples
N_x, N_y, N_{xy} = stress resultants
n = number of circumferential waves
P_{cr}, P_{cr}^* = theoretical critical axial compressive load (P) for perfect and imperfect cylinder, respectively
p_{cr}, p_{cr}^* = theoretical critical pressure (p) for perfect and imperfect cylinder, respectively
q = imperfection axial wave number
q_0 = axisymmetric buckling mode wave number for perfect cylinder $[R(A_{22}^* D_{11}^*)^{-1/2}]^{1/2}$
Q_{11}, Q_{22} = $E_{11}/(1-\nu_{12}\nu_{21})$, $E_{22}/(1-\nu_{12}\nu_{21})$
Q_{12} = $\nu_{21}E_{11}(1-\nu_{12}\nu_{21}) = \nu_{12}E_{22}/(1-\nu_{12}\nu_{21})$
Q_{66} = G_{12}
$\bar{Q}_{11}$ = $Q_{11}C^4 + 2(Q_{12}+2Q_{66})S^2C^2 + Q_{22}S^4$
$\bar{Q}_{22}$ = $Q_{11}S^4 + 2(Q_{12}+2Q_{66})S^2C^2 + Q_{22}C^4$
$\bar{Q}_{12}$ = $(Q_{11}+Q_{22}-4Q_{66})S^2C^2 + Q_{12}(S^4+C^4)$
$\bar{Q}_{66}$ = $(Q_{11}+Q_{22}-2Q_{12}-2Q_{66})S^2C^2 + Q_{66}(S^4+C^4)$
$\bar{Q}_{16}$ = $(Q_{11}-Q_{12}-2Q_{66})SC^3 + (Q_{12}-Q_{22}+2Q_{66})S^3C$
$\bar{Q}_{26}$ = $(Q_{11}-Q_{12}-Q_{66})S^3C + (Q_{12}-Q_{22}+2Q_{66})SC^3$
R = radius of cylinder
R_s, R_p, R_x = T/T_{cr}, p/p_{cr}, P/P_{cr}
$\bar{R}_s, \bar{R}_p, \bar{R}_x$ = T/T_{cr}^*, p/p_{cr}^*, P/P_{cr}^*
S, C = $\sin\theta_k$, $\cos\theta_k$
t = thickness
T_{cr}, T_{cr}^* = theoretical critical torque (T) of perfect and imperfect cylinder, respectively
u, v, w = axial, circumferential, and radial displacements, respectively
x, y, z = axial, circumferential, and radial coordinates, respectively
$\bar{Z}$ = L^2/Rt
$\gamma_{xy}^0, \epsilon_x^0, \epsilon_y^0$ = shear and normal strains with respect to structural axes (x,y)
θ = fiber axis relative to cylinder generator
μ = imperfection amplitude/t

Presented as Paper 78-514 at the AIAA/ASME 19th Structures, Structural Dynamics and Materials Conference, Bethesda, Md., April 3-5, 1978; submitted May 15, 1978; revision received Oct. 10, 1978.

Index categories: Structural Stability; Structural Composite Materials.
*Assistant Professor.
†Professor, Institute for Aerospace Studies. Member AIAA.

Introduction

THE use of composite materials to fabricate load bearing structures is increasing every year. For the case of laminated composite shells, they can exhibit significant buckling sensitivity to geometric shape imperfections similar to that of isotropic shells, particularly for circular cylindrical configurations.[1-4] However, unlike the situation with isotropic structures, the design engineer does have the opportunity to reduce these effects by selecting appropriate laminae orientations.

Previous studies on the buckling of laminated cylinders have been reviewed in Ref. 5. Although more recent investigations based on single load conditions have been published (see Refs. 6 and 7 for example), it would appear that very few combined loading cases have been considered. As early as 1963 Cheng and Ho[8,9] presented an analysis for heterogeneous anisotropic cylinders subject to combined loading, which was later modified by Lei and Cheng[10] for orthotropic laminated cylinders having various boundary conditions. In addition, some experimental results have been reported by Holston et al.[11] for combined torsion/axial compression and bending/axial compression. More recently, combined torsion/axial compression buckling tests were also undertaken by Wilkins and Love[12] and, in both instances, substantial disagreement between theory and experiments was observed.

Because of the anisotropic behavior of laminated cylinders, calculating buckling loads can be a difficult task, especially if one includes boundary conditions, a nonlinear prebuckling state, and shape imperfections. In the following report, interactive buckling under the simultaneous action of axial

compression, external pressure, and torsion is studied. In addition, the effect of an axisymmetric shape imperfection is taken into account, although the experimental data are based on test models containing random imperfection distributions. Due to the infinite number of possible laminae configurations and material systems available, results are presented for only a few cases to demonstrate the effect of fiber orientation, imperfection amplitude, and cylinder length on the interaction behavior.

Theoretical Analysis

The analysis presented in the following sections was based on a nondimensional form of the well-known Donnell-Mushtari-type equations for a circular cylindrical shell containing a small axisymmetric imperfection in shape. Furthermore, the constitutive relations for a thin shell composed of layers of orthotropic material having principal axes oriented in arbitrary directions were employed. Characterizing the external loading (torsion, external pressure, and axial compression) by a single parameter, the method of adjacent equilibrium was used to derive linear equations of neutral stability which, by means of separation of variables, were then reduced to a two-point homogeneous boundary value problem in terms of one independent variable. Nontrivial solutions of the equations yielded eigenvalues, the lowest of which was the value of interest. Restrictions imposed on the analysis required that the external loading be axisymmetric and that the boundary conditions at buckling be symmetric with respect to the midlength of the cylinder.

Basic Equations in Nondimensional Form

The governing equations and boundary conditions are written in the following nondimensional form:

Strain-Displacement Relations‡

$$\bar{\epsilon}_x^0 = (L/t)\,U_{,X} + \tfrac{1}{2}W_{,X}^2 + W_{0,X}W_{,X} \tag{1}$$

$$\bar{\epsilon}_y^0 = (L/t)\,V_{,Y} + \bar{Z}W + \tfrac{1}{2}W_{,Y}^2 \tag{2}$$

$$\bar{\gamma}_{xy}^0 = (L/t)\,U_{,Y} + (L/t)\,V_{,X} + W_{,X}W_{,Y} + W_{0,X}W_{,Y} \tag{3}$$

Equilibrium Equations

$$\bar{N}_{x,X} + \bar{N}_{xy,Y} = 0 \tag{4}$$

$$\bar{N}_{xy,X} + \bar{N}_{y,Y} = 0 \tag{5}$$

$$\bar{M}_{x,XX} + 2\bar{M}_{xy,XY} + \bar{M}_{y,YY} - \bar{Z}\bar{N}_y + \bar{N}_x(W_{0,XX} + W_{,XX}) + 2\bar{N}_{xy}W_{,XY} - \bar{N}_y W_{,YY} + \bar{Z}\bar{p} = 0 \tag{6}$$

Constitutive Relations

$$\begin{bmatrix} \bar{\epsilon}_x^0 \\ \bar{\epsilon}_y^0 \\ \bar{\gamma}_{xy}^0 \\ \bar{M}_x \\ \bar{M}_y \\ \bar{M}_{xy} \end{bmatrix} = \begin{bmatrix} \bar{A}_{11}^* & \bar{A}_{12}^* & \bar{A}_{16}^* & \bar{B}_{11}^* & \bar{B}_{12}^* & \bar{B}_{16}^* \\ \bar{A}_{12}^* & \bar{A}_{22}^* & \bar{A}_{26}^* & \bar{B}_{21}^* & \bar{B}_{22}^* & \bar{B}_{26}^* \\ \bar{A}_{16}^* & \bar{A}_{26}^* & \bar{A}_{66}^* & \bar{B}_{61}^* & \bar{B}_{62}^* & \bar{B}_{66}^* \\ -\bar{B}_{11}^* & -\bar{B}_{21}^* & -\bar{B}_{61}^* & \bar{D}_{11}^* & \bar{D}_{12}^* & \bar{D}_{16}^* \\ -\bar{B}_{12}^* & -\bar{B}_{22}^* & -\bar{B}_{62}^* & \bar{D}_{12}^* & \bar{D}_{22}^* & \bar{D}_{26}^* \\ -\bar{B}_{16}^* & -\bar{B}_{26}^* & -\bar{B}_{66}^* & \bar{D}_{16}^* & \bar{D}_{26}^* & \bar{D}_{66}^* \end{bmatrix} \begin{bmatrix} \bar{N}_x \\ \bar{N}_y \\ \bar{N}_{xy} \\ -W_{,XX} \\ -W_{,YY} \\ -2W_{,XY} \end{bmatrix} \tag{7}$$

Boundary Conditions at $X = \pm 1/2$

$$\bar{N}_x = \bar{N}_x(\pm 1/2, Y) \quad \text{or} \quad U = U(\pm 1/2, Y)$$

$$\bar{N}_{xy} = \bar{N}_{xy}(\pm 1/2, Y) \quad \text{or} \quad V = V(\pm 1/2, Y)$$

$$\bar{M}_x = 0 \quad \text{or} \quad W_{,X} = 0 \tag{8}$$

and $W = 0$, where

$$X = x/L \qquad \bar{M}_x = M_x L^2/D_{11}^* t$$

$$Y = y/L \qquad \bar{M}_y = M_y L^2/D_{11}^* t$$

$$U = u/t \qquad \bar{M}_{xy} = M_{xy} L^2/D_{11}^* t$$

$$V = v/t \qquad \bar{\epsilon}_x^0 = (L/t)^2 \epsilon_x^0$$

$$W = w/t \qquad \bar{\epsilon}_y^0 = (L/t)^2 \epsilon_y^0$$

$$W_0 = w_0/t \qquad \bar{\gamma}_{xy}^0 = (L/t)^2 \gamma_{xy}^0$$

$$\bar{N}_x = N_x L^2/D_{11}^* \qquad \bar{Z} = L^2/Rt$$

$$\bar{N}_y = N_y L^2/D_{11}^* \qquad \bar{A}_{ij}^* = A_{ij}^* D_{11}^*/t^2 \qquad (i,j = 1,2,6)$$

$$\bar{N}_{xy} = N_{xy} L^2/D_{11}^* \qquad \bar{B}_{ij}^* = B_{ij}^*/t \qquad (i,j = 1,2,6)$$

$$\bar{p} = pRL^2/D_{11}^* \qquad \bar{D}_{ij}^* = D_{ij}^*/D_{11}^* \qquad (i,j = 1,2,6) \tag{9}$$

Assumed Imperfection Shape

The initial radial displacement is assumed to be

$$W_0(X) = -\mu \cos \omega X \tag{10}$$

where

$$\omega = 2K[\bar{Z}\bar{A}_{22}^{*\,-1/2}]^{1/2}$$

Reduction of Equations to Two Partial Differential Equations

The analysis is simplified if an Airy stress function $F(X, Y)$ in introduced, which identically satisfies the two equilibrium Eqs. (4) and (5). Through proper substitution (see Ref. 13), the following compact form of the equilibrium and compatibility equations can be derived:

$$\begin{bmatrix} \nabla_A^{4*} & -\nabla_B^{4*} \\ \nabla_B^{4*} & \nabla_D^{4*} \end{bmatrix} \begin{bmatrix} F \\ W \end{bmatrix} = \begin{bmatrix} W_{,XY}^2 - (W_{0,XX} + W_{,XX})W_{,YY} + \bar{Z}W_{,XX} \\ F_{,YY}(W_{0,XX} + W_{,XX}) - 2F_{,XY}W_{,XY} \\ + F_{,XX}W_{,YY} - \bar{Z}F_{,XX} + \bar{Z}\bar{p} \end{bmatrix} \tag{11}$$

‡A comma indicates differentiation with respect to the subscript variables shown.

where

$$\nabla_A^4*(\ ) \equiv \bar{A}_{22}^*(\ )_{,XXXX} - 2\bar{A}_{26}^*(\ )_{,XXXY} + (2\bar{A}_{12}^* + \bar{A}_{66}^*) \times (\ )_{,XXYY} - 2\bar{A}_{16}^*(\ )_{,XYYY} + \bar{A}_{11}^*(\ )_{,YYYY} \tag{12a}$$

$$\nabla_B^4*(\ ) \equiv \bar{B}_{21}^*(\ )_{,XXXX} + (2\bar{B}_{26}^* - \bar{B}_{61}^*)(\ )_{,XXXY} + (\bar{B}_{11}^* + \bar{B}_{22}^* - 2\bar{B}_{66}^*)(\ )_{,XXYY} + (2\bar{B}_{16}^* - \bar{B}_{62}^*)(\ )_{,XYYY} + \bar{B}_{12}^*(\ )_{,YYYY} \tag{12b}$$

$$\nabla_D^4*(\ ) \equiv \bar{D}_{11}^*(\ )_{,XXXX} + 4\bar{D}_{16}^*(\ )_{,XXXY} + 2(\bar{D}_{12}^* + 2\bar{D}_{66}^*) \times (\ )_{,XXYY} + 4\bar{D}_{26}^*(\ )_{,XYYY} + \bar{D}_{22}^*(\ )_{,YYYY} \tag{12c}$$

Stability Equations

Equations of neutral stability can be derived in terms of incremental components of the stress function F and radial displacement W by means of the following relations:

$$F = \hat{F} + \tilde{F}, \quad W = \hat{W} + \tilde{W} \tag{13}$$

where the prebuckling solutions are given by

$$\hat{F}(X, Y) = \tfrac{1}{2}\hat{N}_x Y^2 - \hat{N}_{xy} XY + \hat{f}(X) \tag{14}$$

where

$$\hat{f}_{,XX} = \hat{N}_y = -\left(\frac{\bar{A}_{12}^*}{\bar{A}_{22}^*}\right)\hat{N}_x - \left(\frac{\bar{A}_{26}^*}{\bar{A}_{22}^*}\right)\hat{N}_{xy} + \left(\frac{\bar{Z}}{\bar{A}_{22}^*}\right)\hat{W} + \left(\frac{\bar{B}_{21}^*}{\bar{A}_{22}^*}\right)\hat{W}_{,XX}$$

$$\frac{\hat{N}_x D_{11}^*}{tL^2} = \frac{\hat{N}_x}{t} = \frac{P}{2\pi Rt} = \sigma$$

$$\frac{\hat{N}_{xy} D_{11}^*}{tL^2} = \frac{\hat{N}_{xy}}{t} = \frac{T}{2\pi R^2 t} = \tau$$

and

$$\hat{W}(X) = \begin{cases} B_1 \sinh\lambda_1 X \sin\lambda_2 X + B_2 \cosh\lambda_1 X \cos\lambda_2 X + \hat{W}_P(X) \\ \qquad \text{if } |\hat{N}_X| < |\hat{N}_{X_{cl}}|_A \\ B_1 \sin\lambda_1 X \sin\lambda_2 X + B_2 \cos\lambda_1 X \cos\lambda_2 X + \hat{W}_P(X) \\ \qquad \text{if } |\hat{N}_X| > |\hat{N}_{X_{cl}}|_A \end{cases} \tag{15}$$

depending on the buckling load conditions noted and $|\hat{N}_{X_{cl}}|_A$ corresponds to the classical (perfect cylinder) axial compressive buckling load for the particular shell configuration. It was found that as $\bar{Z}$ was decreased, the latter condition was possible.

$\lambda_1, \lambda_2, B_1$, and B_2 can be determined for a particular set of boundary conditions (see Ref. 13) and

$$\hat{W}_P(X) = \frac{\mu\omega^2 \hat{N}_x}{a_1\omega^4 - a_2\omega^2 + a_3}\cos\omega X + \frac{g_1}{a_3} \tag{16}$$

where

$$a_1 = \bar{B}_{21}^{*2}/\bar{A}_{22}^* + 1$$

$$a_2 = 2\bar{Z}\bar{B}_{21}^*/\bar{A}_{22}^* - \hat{N}_x$$

$$a_3 = \bar{Z}^2/\bar{A}_{22}^*$$

$$g_1 = \bar{Z}(\bar{p} + \bar{A}_{12}^*\hat{N}_x/\bar{A}_{22}^* + \bar{A}_{26}^*\hat{N}_{xy}/\bar{A}_{22}^*)$$

Hence, substituting the expressions for F and W into the compatibility and equilibrium equations yields the following equations for the incremental components:

$$\nabla_A^4*\tilde{F} - \nabla_B^4*\tilde{W} = -g(X)\tilde{W}_{,YY} + \bar{Z}\tilde{W}_{,XX} \tag{17}$$

$$\nabla_B^4*\tilde{F} + \nabla_D^4*\tilde{W} = \hat{N}_x\tilde{W}_{,XX} + g(X)\tilde{F}_{,YY} + 2\hat{N}_{xy}\tilde{W}_{,XY} + \hat{N}_y(X)\tilde{W}_{,YY} - \bar{Z}\tilde{F}_{,XX} \tag{18}$$

where

$$g(X) = W_{0,XX} + \hat{W}_{,XX}$$

Equations (17) and (18) constitute a pair of linear fourth-order homogeneous partial differential equations with variable coefficients. Since the associated boundary conditions in terms of $\tilde{F}$ and $\tilde{W}$ are also linear and homogeneous, the evaluation of critical loads corresponds to an eigenvalue problem.

Recalling the definitions of the differential operators ∇_A^4*, etc., the stability equations can be written as follows:

$$\alpha_1\tilde{F}_{,XXXX} - \alpha_3\tilde{F}_{,XXXY} + \alpha_5\tilde{F}_{,XXYY} - \alpha_7\tilde{F}_{,XYYY} + \alpha_9\tilde{F}_{,YYYY} - \alpha_2\tilde{W}_{,XXXX} - \alpha_4\tilde{W}_{,XXXY} - \alpha_6\tilde{W}_{,XXYY} - \alpha_8\tilde{W}_{,XYYY} - \alpha_{10}\tilde{W}_{,YYYY} = -g(X)\tilde{W}_{,YY} + \bar{Z}\tilde{W}_{,XX} \tag{19}$$

and

$$\alpha_2\tilde{F}_{,XXXX} + \alpha_4\tilde{F}_{,XXXY} + \alpha_6\tilde{F}_{,XXYY} + \alpha_8\tilde{F}_{,XYYY} + \alpha_{10}\tilde{F}_{,YYYY} + \tilde{W}_{,XXXX} + \alpha_{14}\tilde{W}_{,XXXY} + \alpha_{11}\tilde{W}_{,XXYY} + \alpha_{13}\tilde{W}_{,XYYY} + \alpha_{12}\tilde{W}_{,YYYY} = \hat{N}_x\tilde{W}_{,XX} + g(X)\tilde{F}_{,YY} + 2\hat{N}_{xy}\tilde{W}_{,XY} + \hat{N}_y(X)\tilde{W}_{,YY} - \bar{Z}\tilde{F}_{,XX} \tag{20}$$

where expressions for α_i are;

$$\alpha_1 = \bar{A}_{22}^*, \quad \alpha_2 = \bar{B}_{21}^*, \quad \alpha_3 = 2\bar{A}_{26}^*, \quad \alpha_4 = 2\bar{B}_{26}^* - \bar{B}_{61}^*$$

$$\alpha_5 = 2\bar{A}_{12}^* + \bar{A}_{66}^*, \quad \alpha_6 = \bar{B}_{11}^* + \bar{B}_{22}^* - 2\bar{B}_{66}^*, \quad \alpha_7 = 2\bar{A}_{16}^*$$

$$\alpha_8 = 2\bar{B}_{16}^* - \bar{B}_{62}^*, \quad \alpha_9 = \bar{A}_{11}^*, \quad \alpha_{10} = \bar{B}_{12}^*$$

$$\alpha_{11} = 2(\bar{D}_{12}^* + 2\bar{D}_{66}^*), \quad \alpha_{12} = \bar{D}_{22}^*, \quad \alpha_{13} = 4\bar{D}_{26}^*, \quad \alpha_{14} = 4\bar{D}_{16}^* \tag{21}$$

Noting that the remaining coefficients of Eqs. (19) and (20) are functions of X only (except $\bar{Z}$), a solution is possible by means of separation of variables. Hence, the solutions were taken in the form,

$$\tilde{F}_n(X, Y) = F_{1n}(X)\sin\beta_n Y + F_{2n}(X)\cos\beta_n Y \tag{22a}$$

$$\tilde{W}_n(X, Y) = W_{1n}(X)\sin\beta_n Y + W_{2n}(X)\cos\beta_n Y \tag{22b}$$

Reduction of Stability Equations to a Set of Ordinary Differential Equations

Substituting the solutions for $\tilde{F}$ and $\tilde{W}$ given by Eqs. (22) into Eqs. (19) and (20) yields a set of ordinary differential equations in terms of F_1, F_2, W_1, and W_2 for each value of n. These equations were then transformed into a set of 16 first-order differential equations in terms of a general load parameter λ. This was accomplished by assuming the external loads increase proportionally from a point (T_1, p_1, P_1) in three-dimensional load space to another point (T, p, P)

whereby

$$T/T_1 = p/p_1 = P/P_1 = \lambda \tag{23}$$

Critical combinations of load $(T, p, P)_{cr}$ define a stability or interaction surface in the load space.

A numerical technique known as the "multisegment" method[14] was used to solve the homogeneous boundary value problem. Satisfaction of the particular boundary conditions required the characteristic determinant to vanish. Consequently, by varying the wave number n, the lowest eigenvalue (λ_{cr}) was selected as the critical buckling parameter.

Theoretical Results

Critical combinations of torsion, external lateral pressure, and axial compression were evaluated for several laminate configurations based on a clamped end constraint. The results are presented in terms of the nondimensional load ratios.

Perfect Anisotropic Cylinders

Since there are an infinite number of possible laminate configurations, the numerical calculations were, for the most part, limited to a $(\theta, 0, -\theta)$ glass/epoxy composite cylinder with laminae of equal thickness. Results were obtained for a value of $\bar{Z} = 200$, and both positive and negative torque were taken into account. The resulting interaction curves are plotted in Figs. 1-3 for varying values of θ.

For anisotropic cylinders, $\bar{N}_{xy_{cr}}$ (T_{cr}) was defined as the critical shear stress (torque) corresponding to positive (clockwise) torsional loading. When $R_P = R_x = 0$,

$$R_s = \begin{cases} 1 & \text{for positive applied torque} \\ \dfrac{\bar{N}_{xy_{\text{neg}}}}{\bar{N}_{xy_{cr}}} = \dfrac{T_{\text{neg}}}{T_{cr}} & \text{for negative applied torque} \end{cases} \tag{24}$$

In fact, it appears that small values of negative torque can stabilize the cylinder, as demonstrated by the axial compression loads (R_x) being slightly higher in value than the load corresponding to zero applied torque (see Fig. 2).

One interesting feature relates to the inclusion of nonlinear prebuckling deformations in the analysis. Present theoretical results for buckling under pure axial compression and those obtained from a linear-type analysis for a $(\theta, 0, -\theta)$ glass/epoxy composite cylinder are compared in Fig. 4. Depending on the fiber orientation, the predictions of the two theories can differ by as much as 15%. This is attributed to the fact that the analysis of Ref. 3 neglects nonlinear prebuckling deformations associated with end constraints and assumes an approximate buckling mode shape.

As shown in Figs. 1-3, the interaction curves for a $(\theta, 0, -\theta)$ glass/epoxy cylinder can vary significantly in shape for $0 \le \theta \le 90$ deg. Consequently, for each value of θ, the interaction surfaces based on "exact" theory were approximated by the following formula:

$$\begin{aligned} &F_1 R_s + F_2 R_P + F_3 R_x + (1 - F_1) R_s^2 + (1 - F_2) R_P^2 \\ &\quad + (1 - F_3) R_x^2 + 2F_{12} R_s R_P + 2F_{13} R_s R_x \\ &\quad + 2F_{23} R_P R_x - 1 = 0 \end{aligned} \tag{25}$$

where

$$F_1 = 1 + \bar{N}_{xy_{cr}} / \bar{N}_{xy_{\text{neg}}}$$

The resulting sets of coefficients (F) were determined by a least squares fit to the numerical results and are given in Table 1 for several values of θ.

Imperfect Anisotropic Cylinders

The computations for the glass/epoxy $(\theta, 0, -\theta)$ axisymmetric imperfect cylinders were performed for values of $K = 1/2$ and $\mu = 0.1$. Note that the selection of $K = 1/2$ corresponds to an axisymmetric imperfection having the form of the classical axial compressive buckling mode.

Based on these calculations, it was found that this imperfection mode had little effect on buckling under external pressure on torsion in that the interaction curves obtained did not differ significantly from those shown in Fig. 3. However, the degradation was most pronounced when axial com-

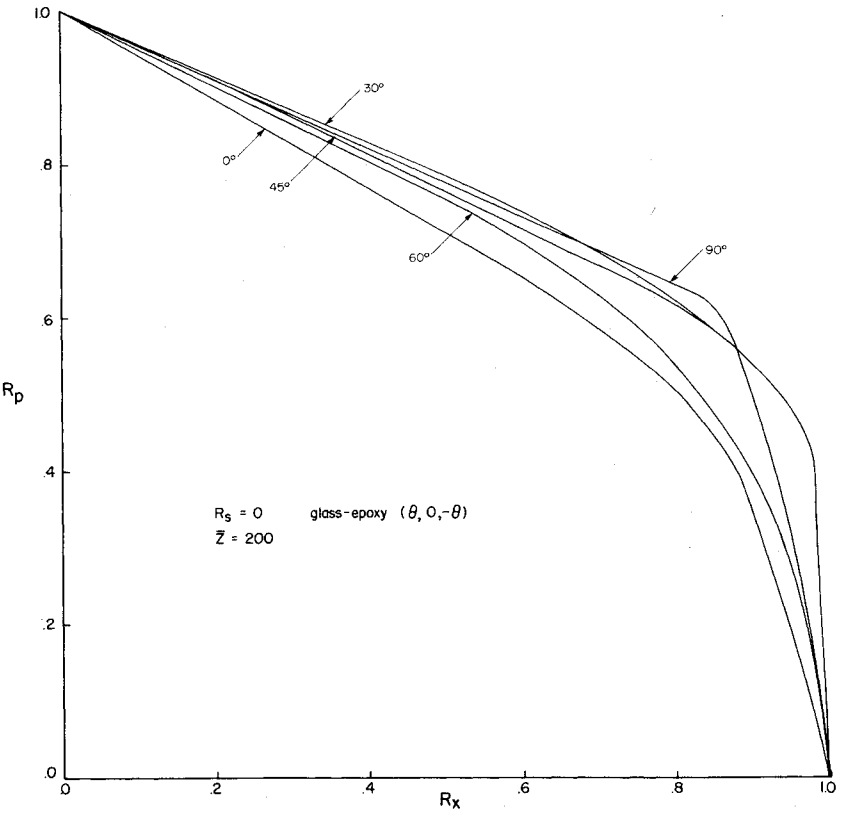

Fig. 1 Critical combinations of external lateral pressure and axial compression for perfect composite cylinder (theory).

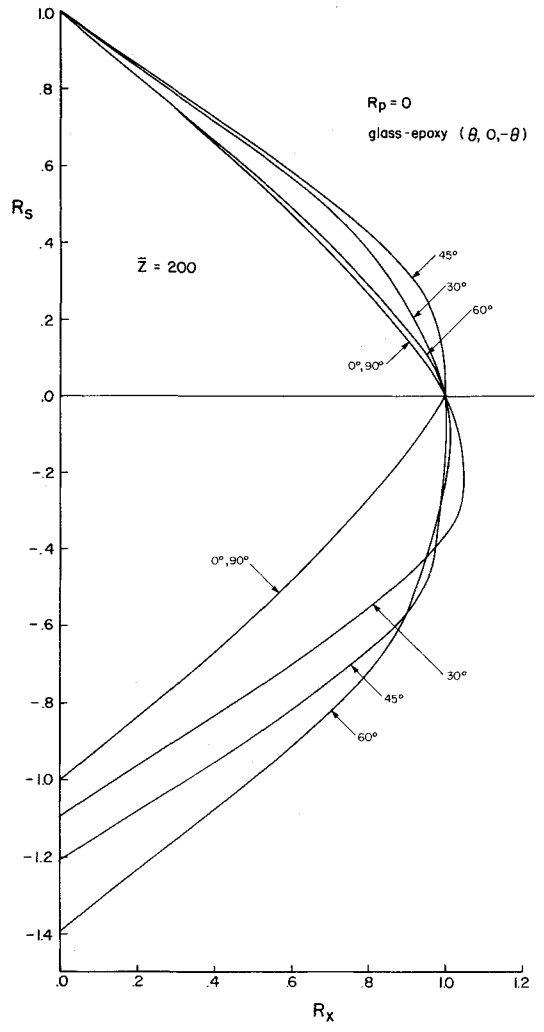

Fig. 2 Critical combinations of torsion and axial compression for perfect composite cylinder (theory).

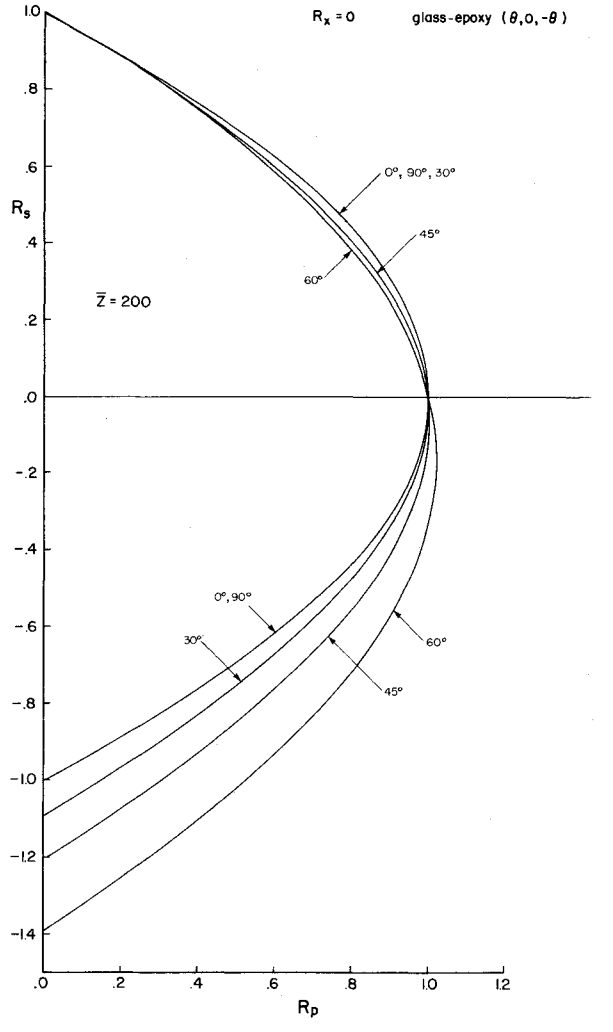

Fig. 3 Critical combination of torsion and external lateral pressure for perfect composite cylinder (theory).

pression was present, as is evident when one compares the interaction curves of Figs. 5 and 6 with those in Figs. 1 and 2. From a design viewpoint, substantially higher interactive buckling strengths can result by the proper selection of fiber orientations, even when one takes into account the presence of shape imperfections. This is readily seen when one compares the magnitude of the load vectors in Figs. 5 and 6.

Effect of Varying $\bar{Z}$

For sufficiently large values of $\bar{Z}$, it was of interest to determine if simple relations similar to those for isotropic cylinders could be utilized to compute buckling loads, viz,

$$\bar{N}_{xy_{cr}} = \bar{C}_s \bar{Z}^{3/4} \tag{26a}$$

$$\bar{p}_{cr} = \bar{C}_P \bar{Z}^{1/2} \tag{26b}$$

$$\bar{N}_{x_{cr}} = \bar{C}_x \bar{Z} \tag{26c}$$

where $\bar{C}_s$, $\bar{C}_P$, $\bar{C}_x$ depend on the prescribed boundary conditions and on laminate properties, but are hopefully independent of $\bar{Z}$. To test the accuracy of these equations for more arbitrary laminate configurations, a graphite/epoxy (−10, 20, 70) laminate was investigated. This particular configuration led to a fully populated constitutive matrix and, as a result, significant anisotropy. Values of $\bar{N}_{xy_{cr}}$, $\bar{p}_{cr}$, and $\bar{N}_{x_{cr}}$ were obtained for $\bar{Z}=200$ and 1000 (Table 2). By comparing these values with the predicted results from Eq. (26), it was found that agreement within 5% was achieved.

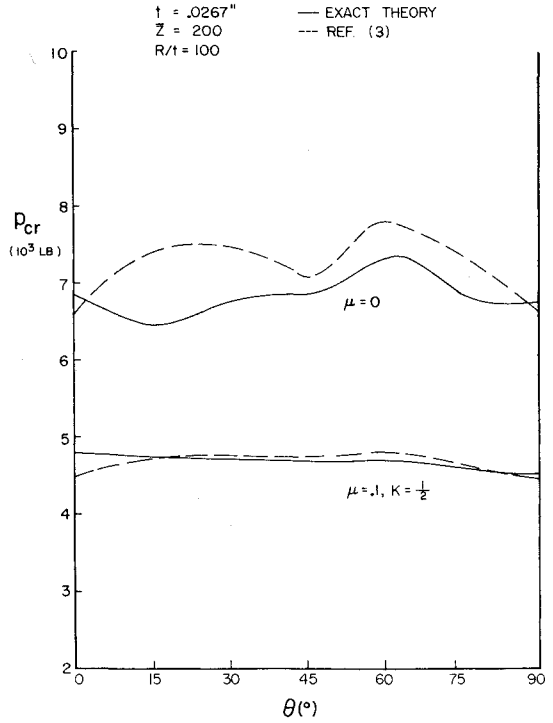

Fig. 4 Buckling loads of axially compressed perfect and imperfect glass/epoxy composite cylinders (θ, 0, $-\theta$).

Table 1 Perfect glass/epoxy $(\theta,0,-\theta)$ composite cylinder interaction surface coefficients

θ, deg	F_1	F_2	F_3	F_{12}	F_{13}	F_{23}
0	0	1.078	1.721	0	0	−0.5558
30	0.08592	1.056	1.265	−0.03025	0.06780	−0.4869
45	0.1742	1.066	1.161	−0.02518	0.01175	−0.4712
60	0.2806	1.022	1.362	−0.02208	−0.00304	−0.4657
90	0	1.033	1.611	0	0	−0.5285

Table 2 Graphite/epoxy (−10,20,70) composite cylinder
$R/t = 100$, $\mu = 0$, $E_{11} = 20\times10^6$ psi, $E_{22} = 1\times10^6$ psi, $\nu_{12} = 0.25$, $G_{12} = 0.6\times10^6$ psi

$\bar{Z}$	$\bar{N}_{xy_{cr}}$	$\hat{p}_{cr}$	$\bar{N}_{x_{cr}}$	$\bar{N}_{xy_{cr}}/\bar{Z}^{3/4}$	$\hat{p}_{cr}/\bar{Z}^{1/2}$	$\bar{N}_{x_{cr}}/\bar{Z}$
200	423.5	173.7	−828.8	7.96	12.28	4.14
1000	1345	395.4	−4144	7.563	12.50	4.14

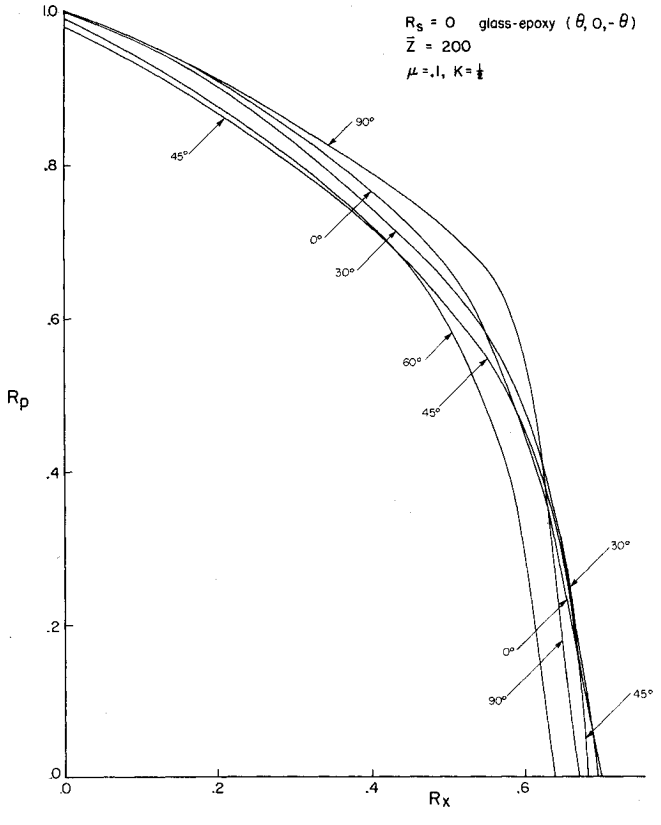

Fig. 5 Critical combinations of external lateral pressure and axial compression for imperfect composite cylinder (theory).

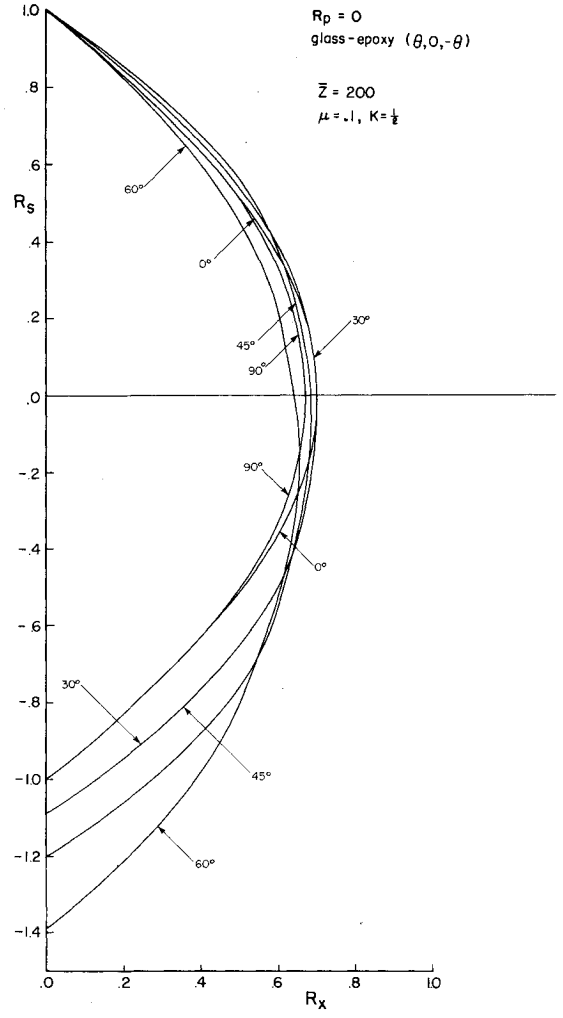

Fig. 6 Critical combinations of torsion and axial compression for imperfect composite cylinder (theory).

Of considerable importance is the effect of small $\bar{Z}$ on both the individual buckling loads and the corresponding interaction diagrams. From earlier studies for isotropic cylinders (see Ref. 15), it was shown that as $\bar{Z}\to20$, the axial compression-lateral pressure interaction curves changed from concave to convex (as viewed from the origin). Similar interaction behavior has been found for a laminated composite cylinder (see Fig. 7), although more analysis is required since this phenomenon may not necessarily occur for other load combinations. One should also note that linear theory will not predict the "concave" interaction curve and recourse to the nonlinear prebuckling state solution must be made.

Comparison with Experiment: Combined Loading Buckling Tests

Torsional loading was applied by means of two calibrated Scheffer hydraulic pistons controlled by oil pressure. Each of the pistons was attached to opposite ends of a plate securely bolted to the top end plate of the shell so that a torsional couple could be applied about the cylinder axis. The piston blocks were firmly attached to rigid supports secured to the Tinius Olson testing machine. Pressure was applied to the pistons by means of a hand pump and readings were taken from pressure gages.

External hydrostatic pressure was applied by partially evacuating the inside of the shell which was sealed at the top by the end plate and at the bottom by means of an O-ring

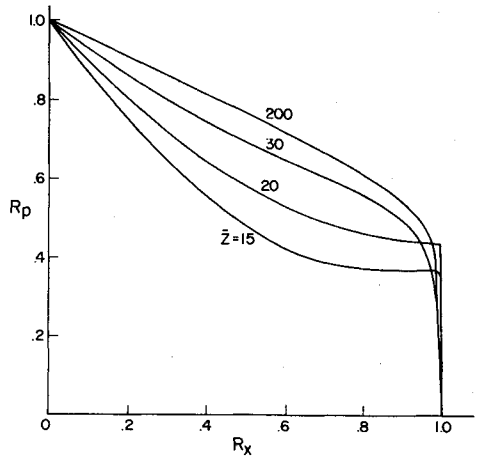

Fig. 7 Effect of $\bar{Z}$ on interactive buckling behavior for laminated cylinder [glass/epoxy, (45 deg., 0 deg, −45 deg), $R/t = 100$].

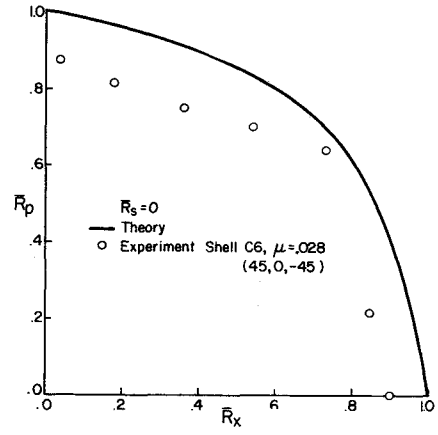

Fig. 9 Critical combinations of external pressure and axial compression for an imperfect glass/epoxy composite cylinder.

fitted between the open end plate and a base plate bolted to the Tinius Olson machine. Air was evacuated by means of a vacuum pump-reservoir system. For this purpose, an outlet had been machined radially through the base plate and up to the inside of the shell. The testing procedure consisted of evacuating the reservoir, shutting off the vacuum pump, and then slowly opening a sensitive pressure regulator until the desired value of external pressure was reached. Pressures were converted to electrical signals by means of a calibrated Schaevitz LVDT-type pressure transducer in conjunction with an X-Y plotter.

Uniform axial end load was applied with the Tinius Olson testing machine. An additional check of uniformity of axial stress was made by observing the postbuckled configuration, insuring that buckling occurred completely around the circumference.

To allow rotation of the top end of the cylinder under torsional loading, a thrust bearing was inserted between the load platen of the testing machine and the top end plate of the cylinder. Simultaneous loading with torsion, external hydrostatic pressure, and axial compression was accomplished by first preloading the cylinder with one or two types of load and then slowly increasing the remaining load until buckling occurred. In all cases, buckling was accompanied by a visible snap-through and a subsequent drop in load. Buckling tests were found to be repeatable and, for the few cases checked, changing the order of loading did not have a significant effect. Thus, the buckling loads obtained were regarded as essentially independent of load sequence. Consequently, although the method of loading did not conform to Eq. (23), this was assumed to have a negligible influence on the buckling comparison with theory.

The experiments consisted of buckling two, three-ply laminated glass/epoxy (Scotchply XP250) preimpregnated tape wound cylinders supplied by the Structures Division of the Flight Dynamics Laboratory, Wright-Patterson Air Force Base. Since these shells were of the same type used in Ref. 4, the corresponding material properties were assumed for shell C1 (−70, 70, 0) and shell C6 (45, 0, −45). All experiments were conducted in the linear elastic range of the material.

Each cylinder was clamped at the ends with aluminum end plates bonded to the shell wall with an epoxy plastic. The

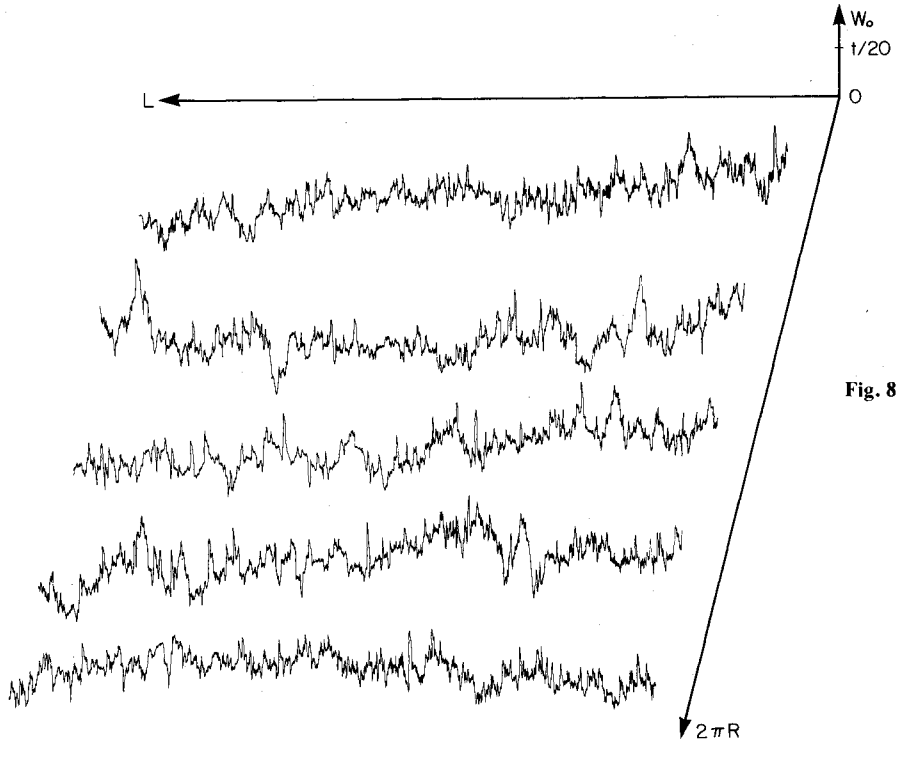

Fig. 8 Median surface profiles for composite shell C6.

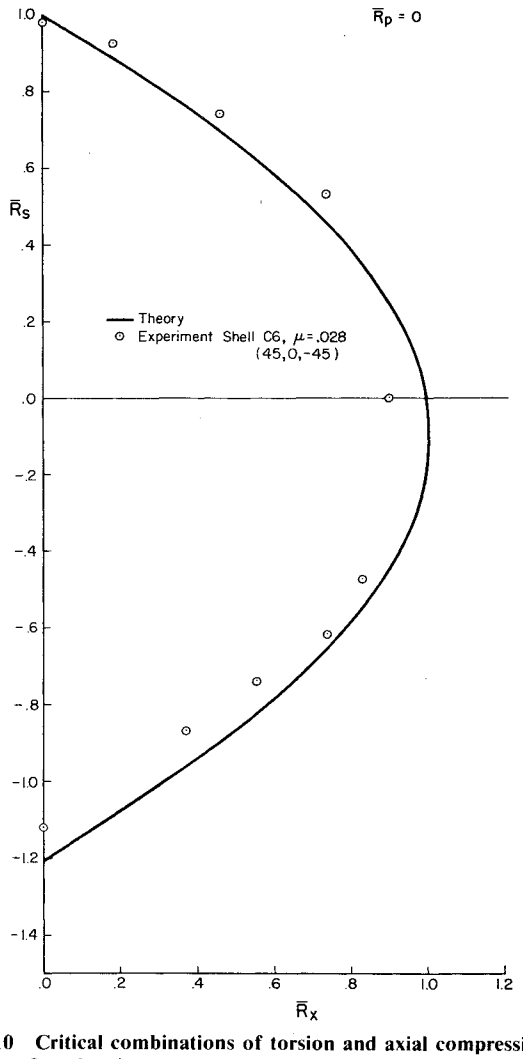

Fig. 10 Critical combinations of torsion and axial compression for an imperfect glass/epoxy composite cylinder.

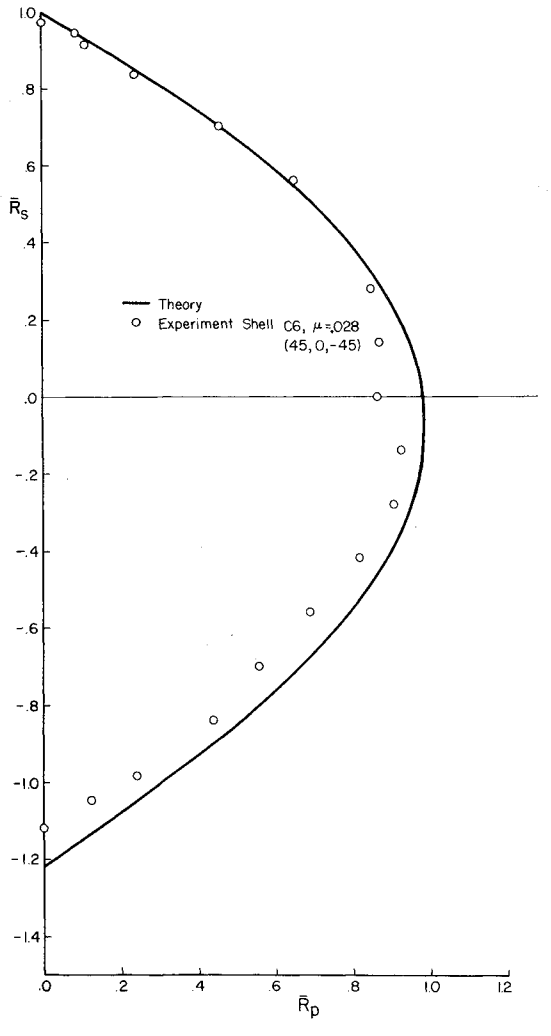

Fig. 11 Critical combinations of torsion and external pressure for an imperfect glass/epoxy composite cylinder.

bottom end plate was actually a ring, permitting the cylinder to be placed over an internal mandrel which was used to prevent excessive postbuckling deformations and subsequent fracture. As a result, repeatable testing was possible.

Due to the method of manufacture, the shells contained unintentional random shape imperfections, as shown in Fig. 8. These imperfection distributions were obtained using a profile measuring apparatus consisting of two opposing, low-pressure contact displacement transducers. Both thickness data and median surface profiles were obtained in this manner (see Ref. 4 for more details). Since the imperfection distribution was clearly not axisymmetric, the procedure proposed in Ref. 4 was adopted. This approach employs a root-mean-square imperfection amplitude (determined from the actual profile measurements) together with the critical axisymmetric buckling mode wavelength of the specific cylinder to generate an equivalent deterministic imperfection. It may be pointed out that one could also use the critical asymmetric square wave mode with equal justification. Hence, the root-mean-square value of the imperfection (initial radial displacement) was evaluated for each of several generators and the largest value (δ_{rms}) was then used to calculate an equivalent axisymmetric imperfection amplitude, $\mu = \sqrt{2}\,\delta_{\text{rms}}/t$.

Using the approximate interaction formulas for the (-70, 70, 0) and (θ, 0, $-\theta$) glass/epoxy cylinders, a comparison between experiment and theory was possible (assuming that the coefficients F_1, F_2, F_3, etc., are approximately independent of $\bar{Z}$ for $\bar{Z} > 200$). These coefficients were then evaluated for the appropriate values of μ and the resulting interaction curves are shown in Figs. 9-16. Note that the load ratios are expressed in terms of the imperfect cylinder buckling values. The experimental data for both shell structures are also included for comparison purposes and it

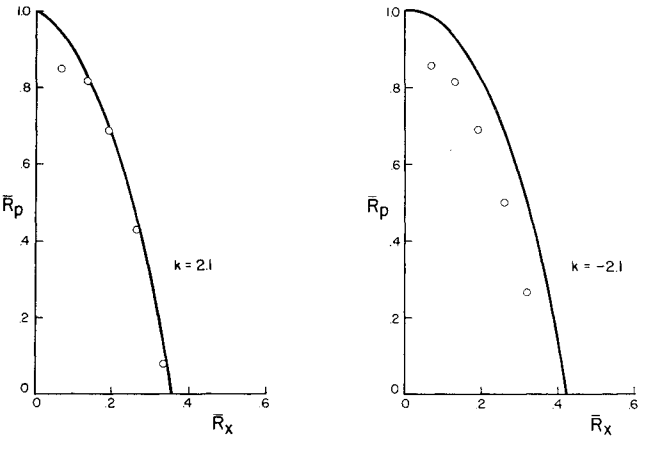

Fig. 12 Critical combinations of torsion, external pressure and axial compression for an imperfect glass/epoxy composite cylinder, $\bar{R}_s = k\bar{R}_x$; ——— theory, o experiment; shell—C6, $\mu = 0.028$ (45 deg, 0 deg, −45 deg).

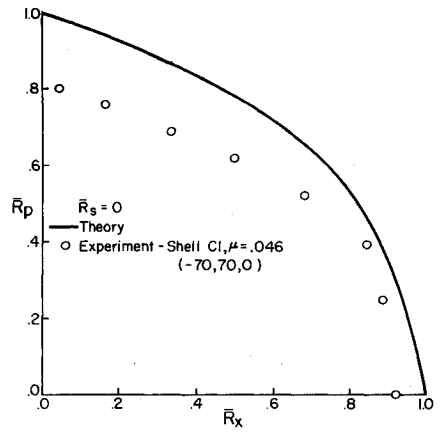

Fig. 13 Critical combinations of external pressure and axial compression for an imperfect glass/epoxy composite cylinder.

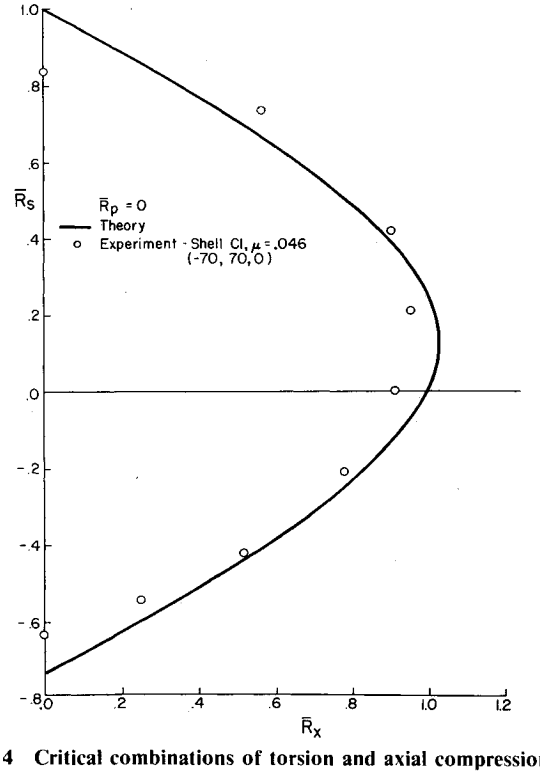

Fig. 14 Critical combinations of torsion and axial compression for an imperfect glass/epoxy composite cylinder.

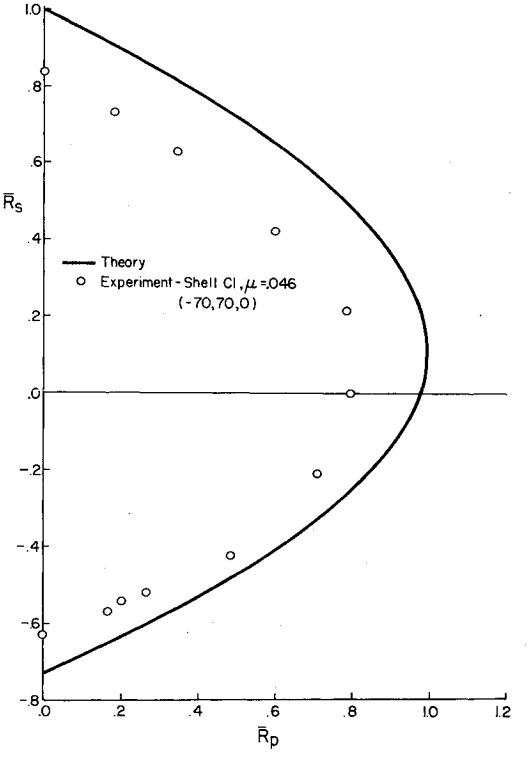

Fig. 15 Critical combinations of torsion, external pressure, and axial compression of an imperfect glass/epoxy composite cylinder.

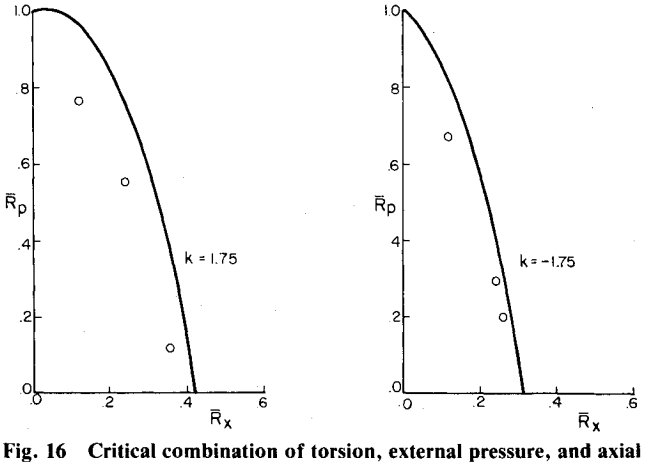

Fig. 16 Critical combination of torsion, external pressure, and axial compression for an imperfect glass/epoxy composite cylinder $\bar{R}_s = k\bar{R}_x$; — theory, o experiment; shell C1, $\mu = 0.046$ (−70, 70, 0).

can be seen that reasonably good correlation was obtained, bearing in mind the presence of random imperfections in the cylinders. Figures 12 and 16 were included to demonstrate buckling under three simultaneous loads where, in each case, the experimental load ratio $k = \bar{R}_s / \bar{R}_x$ was held constant.

Conclusions

Theoretical results based on a nonlinear prebuckling state have been presented demonstrating the effect of varying fiber angle on the interactive buckling behavior of geometrically "perfect" and axisymmetric imperfect laminated composite circular cylinders. The shape of the interaction curves has been shown to vary significantly for different laminate configurations. In addition, as the $\bar{Z}$ parameter was decreased, the interaction curves for pressure/compression loading changed from concave to convex, thus negating the "conservative" linear interaction design criterion.

Buckling experiments, which were carried out on cylinders containing random geometric shape imperfection distributions, were found to agree reasonably well with predictions using the largest measured rms imperfection amplitude and the critical axisymmetric buckling mode (i.e., $K = \frac{1}{2}$). From a design viewpoint, the notion of calculating buckling loads on the basis of an "equivalent" deterministic imperfection (in this case, an axisymmetric mode) seems to account for the reductions in buckling strength associated with the presence of small-amplitude random imperfections (i.e., of the order of the wall thickness or less) for moderately long cylinders. In the absence of more extensive imperfection profile data, it is proposed that this method of buckling analysis be considered.

Acknowledgment

The authors wish to acknowledge the financial support of this research program by the National Research Council of Canada under Grant A-2783. The glass fiber reinforced

cylinders were supplied by the Structures Division of the Flight Dynamics Laboratory, Wright-Patterson Air Force Base, courtesy of N. Khot.

References

[1] Card, M. F., "The Sensitivity of Buckling of Axially Compressed Fiber-Reinforced Cylindrical Shells to Small Geometric Imperfections," NASA TMX-61914, June 1969.

[2] Khot, N. S., "Buckling and Postbuckling Behavior of Composite Cylindrical Shells Under Axial Compression," *AIAA Journal*, Vol. 8, Feb. 1970, pp. 229-235.

[3] Tennyson, R. C., Chan, K. H., and Muggeridge, D. B., "The Effect of Axisymmetric Shape Imperfections on the Buckling of Laminated Anisotropic Circular Cylinders," *Canadian Aeronautics and Space Institute, Transactions*, Vol. 4, Sept. 1971, p. 131.

[4] Tennyson, R. C. and Muggeridge, D. B., "Buckling of Laminated Anisotropic Imperfect Circular Cylinders Under Axial Compression," *Journal of Spacecraft and Rockets*, Vol. 10, Feb. 1973, pp. 143-148.

[5] Tennyson, R. C., "Buckling of Laminated Composite Cylinders: A Review," *Composites* (U.K.), Jan. 1975.

[6] Jones, R. M. and Morgan, H. S., "Buckling and Vibration of Cross-Ply Laminated Circular Cylindrical Shells," *AIAA Journal*, Vol. 13, May 1975, pp. 664-671.

[7] Jones, R. M. and Hennemann, J.C.F., "Effect of Prebuckling Deformations on Buckling of Laminated Composite Circular Cylindrical Shells," *Proceedings of AIAA 19th Structures, Structural Dynamics and Materials Conference*, Bethesda, Md., April 1978.

[8] Cheng, S. and Ho, B.P.C., "Stability of Heterogeneous Aeolotropic Cylindrical Shells Under Combined Loading," *AIAA Journal*, Vol. 1, April 1963, pp. 892-898.

[9] Ho, B.P.C. and Cheng, S., "Some Problems in Stability of Heterogeneous Aeolotropic Cylindrical Shells Under Combined Loading," *AIAA Journal*, Vol. 1, July 1963, pp. 1603-1607.

[10] Lei, M. M. and Cheng, S., "Buckling of Composite and Homogeneous Isotropic Cylindrical Shells Under Axial and Radial Loading," *Journal of Applied Mechanics, Transactions of ASME*, Dec. 1969.

[11] Holston, A. Jr., Feldman, A., and Stang, D. A., "Stability of Filament-Wound Cylinders Under Combined Loading," Air Force Dynamics Laboratory, Wright-Patterson Air Force Base, Ohio, AFFDL-TR-67-55, May 1967.

[12] Wilkins, D. J. and Love, T. S., "Combined Compression-Torsion Buckling Tests of Laminated Composite Cylindrical Shells," *Proceedings of AIAA 15th Structures, Structural Dynamics and Materials Conference*, Las Vegas, Nev., April 1974.

[13] Booton, M., "Buckling of Imperfect Anisotropic Cylinders Under Combined Loading," University of Toronto, Institute for Aerospace Studies, Rept. No. 203, Aug. 1976.

[14] Kalnins, A., "Analysis of Shells of Revolution Subject to Symmetric and Nonsymmetric Loads," *Journal of Applied Mechanics, Transactions of ASME*, Vol. 31, Sept. 1964.

[15] Tennyson, R. C., Booton, M., and Chan, K. H., "Buckling of Short Cylinders Under Combined Loading," *Journal of Applied Mechanics, Transactions of ASME*, Vol. 45, Sept. 1978.